An in Situ Study of Mesostructured CTAB−Silica Film Formation during Dip Coating Using Time-Resolved SAXS and Interferometry Measurements

David Grosso,*,† Florence Babonneau,† Pierre-Antoine Albouy,‡ Heinz Amenitsch,§ A. R. Balkenende,|| Aline Brunet-Bruneau,⊥ and Josette Rivory⊥

Chimie de la Matière Condensée, UPMC−CNRS, 4 place Jussieu, 75005 Paris, France, Laboratoire de Physique des Solides, Université Paris-Sud, 91405 Orsay, France, Institute of Biophysics and X-ray Structure Research, Austrian Academy of Sciences, Steyrergasse 17/VI, 8010 Graz, Austria, Philips Research Laboratories, Prof. Holstlaan 4, 5656 AA Eindhoven, Netherlands, and Laboratoire d'Optique des Solides, UPMC, 4 place Jussieu, 75 252 Paris, France

Received October 11, 2001

Silica thin films with ordered porosity can be prepared by dip coating, combining polycondensation of silicate species and organization of amphiphilic mesophases. This paper reports on the preparation of templated films using cetyltrimethylammonium bromide (CTAB) as the surfactant and tetraethoxysilane (TEOS) as the inorganic precursor. Depending on the CTAB/Si molar ratio, films with different porous networks—3D hexagonal ($P6_3/mmc$), cubic ($Pm3n$), and columnar hexagonal ($p6m$)—were obtained. Identification of the structures was accomplished by coupling two-dimensional X-ray diffraction at grazing incidence and TEM investigations on film cross sections. Other experimental parameters (e.g., deposition rate and composition of the starting sol, including its aging time) appeared also to influence the degree of organization of the final films greatly. To obtain a better understanding of the self-assembly mechanism, the structural formation of the films was followed in real time by in situ SAXS. Because of the very fast self-assembly process (<30 s), high-flux synchrotron radiation was used, which allows to record good quality X-ray patterns in 100 ms. For the first time, interferometry measurements were also combined with the SAXS experiments to correlate the organization steps detected during dip coating with the thickness profiles. A model has thus been proposed for the film formation: organization at the mesoscale (i) takes place at the final stage of liquid-phase evaporation; (ii) involves the formation of micelles at the film/air interface in the early stage of deposition and, in some cases, the formation of intermediate phases; and (iii) is influenced by the condensation degree of inorganic intermediates, the surfactant concentration, and the deposition external conditions.

1. Introduction

The synthesis of mesostructured materials involves the formation of organic−inorganic composites by a self-assembly process, whereby the organic phase is organized on a mesoscopic scale and serves as a template for the inorganic skeleton.[1−3] Mesoporous silica films with various structures are attracting growing interest because of their possible applications in the fields of optics, catalysis, and separation. The first reported studies concerned the growth of mesoporous films at water/air[4] or water/mica[5] interfaces. This long sedimentation process resulted in films that were continuous but macroscopically inhomogeneous on micrometer length scales. Better homogeneity and optical quality can be obtained through liquid deposition techniques such as spin and dip coating.[6−16] With such synthetic methods,

* Author to whom correspondence should be addressed.
† Chimie de la Matière Condensée, UPMC−CNRS.
‡ Université Paris-Sud.
§ Austrian Academy of Sciences.
|| Philips Research Laboratories.
⊥ Laboratoire d'Optique des Solides, UPMC.

(1) Beck, J. S.; Vartuli, J. C.; Roth, W. J.; Leonovicz, M. E.; Kresge, C. T.; Shimtt, K. D.; Chu, C. T−W.; Olson, D. H.; Sheppard, E. W.; McCullen, S. B.; Higgins, J. B.; Schlenker, J. L. *J. Am. Chem. Soc.* **1992**, *114*, 10834.
(2) Ying, J. Y.; Mehnert, C. P.; Wong, M. S. *Angew. Chem., Int. Ed.* **1999**, *38*, 56.
(3) Barton, T. J.; Bull, L. M.; Klemperer, W. G.; Loy, D. A.; McEnaney, B.; Misono, M.; Monson, P. A.; Pez, G.; Scherer, G. W.; Vartuli, J. C.; Yaghi, O. M. *Chem. Mater.* **1999**, *11*, 2633.
(4) Yang, H.; Coombs, N.; Sokolov, I.; Ozin, G. A. *Nature* **1996**, *381*, 549.
(5) Yang, H.; Kuperman, A.; Coombs, N.; Mamiche-Afara, S.; Ozin, G. A. *Nature* **1996**, *379*, 703.
(6) Zhao, D.; Yang, P.; Margolese, D. I.; Chmelka, B. F.; Stucky, G. D. *Chem. Commun.* **1998**, 2499.
(7) Lu, Y.; Ganguli, R.; Drewien, C. A.; Anderson, M. T.; Brinker, C. J.; Gong, W.; Guo, Y.; Soyez, H.; Dunn, B.; Huang, M. H.; Zink, J. I. *Nature* **1997**, *389*, 364.
(8) Zhao, D.; Yang, P.; Melosh, N.; Feng, J.; Chmelka, B. F.; Stucky, G. D. *Adv. Mater.* **1998**, *10*, 1380.
(9) Klotz, M.; Ayral, A.; Guizard, C.; Cot, L. *J. Mater. Chem.* **2000**, *10*, 663.
(10) Grosso, D.; Balkenende, A. R.; Albouy, P. A.; Lavergne, M.; Babonneau, F. *J. Mater. Chem.* **2000**, *10*, 2085.
(11) Besson, S.; Gacoin, T.; Jacquiot, C.; Ricolleau, C.; Babonneau, D.; Boilot, J.-P. *J. Mater. Chem.* **2000**, *10*, 1331.
(12) Kundu, D.; Zhou, H. S.; Honma, I. *J. Mater. Sci. Lett.* **1998**, *17*, 2089.

10.1021/cm011255u CCC: $22.00
Published on Web 01/11/2002

a large variety of silica film structures have been obtained with micellar interconnected pores (3D hexagonal or cubic structures),[6−8,10,11,17] columnar noninterconnected pores (*p*6*m* hexagonal structure[6,8,9]) or lamellar structures.[7,12] In such a template approach, a self-assembly process occurs between the surfactant and the inorganic silica phase, leading to the final mesostructured hybrid material. The formation of the final structure is governed by the shape of the micelles present in solution, the surfactant concentration, the nature of the interactions at the micelle/sol interface, and the morphology of the inorganic intermediate moieties. However, the self-assembly mechanism that drives both organic and inorganic phases to coexist in a well-defined mesostructure within the final material is far from being well understood.

The formation of mesostructured films by dip coating implies experimental conditions that are somehow different from those used to produce bulk materials. The preparation of high-optical-quality thin films requires a low silicate precursor condensation rate and a homogeneous wetting of the selected substrates. Therefore, for silica-based films, initial solutions containing a small amount of water are highly diluted in a solvent such as an alcohol that exhibits good wettability properties toward the substrates (usually glass or silicon wafer). Mildly acidic catalysis, which leads to transparent gels, does not promote extensive silicate condensation and is thus preferred. Once the wet film is deposited, the formation of the mesostructure takes place within the film via evaporation-induced self-assembly.[18] As a result, several mechanisms compete during a very short period of time: evaporation of solvent, self-assembly of organic and inorganic species, organization in mesophases, and polycondensation of the silica network. The solvent, followed by the water, departs from the film/air interface,[19] inducing gradients of concentration in the film thickness and with drying time. The advancement of the self-assembly and organization processes is therefore expected, at any given time, to vary depending on the regions of the layer. To obtain homogeneous structured mesoporous films, it is necessary that the formation of the mesophase occurs when the polycondensation of the inorganic species is not too advanced.[9,18,19] Indeed, in our systems, we will show, by coupling XRD and ^{29}Si NMR experiments, that the formation of well-organized structures requires an optimal degree of condensation for the silicate species in the initial solution. With such complex simultaneously competing reactions, it is a real challenge to understand the different steps involved in the formation of the mesostructured films and to possibly obtain, in the future, better control of the film structure.

The only attempt to follow in situ film formation was performed by the combination of interferometry and luminescence spectroscopy.[7,19,20] These optical techniques have already been used to characterize the drying of surfactant-free silica film.[21,22] They provide valuable information on the film thickness or on the mobility of the species in the film but cannot provide any insights into the organization of templated films. As a result of the rapid formation process of the films, it is impossible to obtain such time-resolved structural information with conventional X-ray diffraction (XRD) equipment as the acquisition time is far too long compared to the evaporation time. A few interesting studies, performed with high-flux small angle X-ray scattering (SAXS) beamlines, on the kinetics of surfactant-silicate phase behavior during the preparation of powdered samples, have recently been published,[23−26] but when this project started, no similar investigations on films had been attempted. By adapting a dip coater on a SAXS beamline, we were able to record a XRD pattern of the drying film every 100 ms during the first minutes of the deposition process. In parallel, the evolution of the film thickness profile with time during dip coating was followed using interferometry and ellipsometry. A comparison between the evolution of the film thickness and film structure deduced by SAXS measurements shows that micelles form first at the air/film interface, whereas the final film structure develops when most of the liquid phase has already departed from the film.

2. Experimental Section

A prehydrolyzed solution was prepared by refluxing for 1 h an ethanolic solution containing TEOS, deionized water, and hydrochloric acid in the molar ratio of 1 TEOS:3 EtOH:5 × 10^{-5} HCl:1 H_2O. A second solution obtained by dissolution of CTAB in ethanol was then added to the prehydrolyzed solution, together with an additional amount of water and HCl. Typical molar ratios were 1 TEOS:20 EtOH:0.004 HCl:2−10 H_2O:0.8−0.14 CTAB. The templated films were prepared by dip coating silicon wafers in the solutions previously aged for 1 week. Micrographs of film cross sections were obtained with a transmission electron microscope (TEM) JEOL 100 CXII apparatus. The ^{29}Si solution-state NMR spectra were recorded on a MSL400 spectrometer at 79.5 MHz, with a pulse width of 12.8 μs and recycle delays of 60 s. The Si sites are labeled Q_n, where n represents the number of oxo bridges bonded to the observed sites. $\theta-2\theta$ X-ray diffractograms of the films were recorded with a conventional PW 1820 Philips goniometer, using Cu Kα radiation (acquisition time of 1 s per 0.005° step).

Time-resolved SAXS measurements were performed at the Austrian high-flux SAXS beamline of the 2-GeV electron storage ring ELETTRA in Trieste, Italy.[27] A dip coater was specifically designed to fit the SAXS beamline. Usually, the substrate was dipped into the container filled with the sol and

(13) Ogawa, M. *Langmuir* **1997**, *13*, 1853.
(14) Ogawa, M.; Ishikawa, H.; Kikuchi, T. *J. Mater. Chem.* **1998**, *8*, 1783.
(15) Martin, J. M.; Anderson, M. T.; Odinek, J.; Newcomer, P. *Langmuir* **1997**, *13*, 4133.
(16) Honma, I.; Shen Zhou, H.; Kundu, D.; Endo, A. *Adv. Mater.* **2000**, *12*, 1529.
(17) Zhao, D.; Huo, Q.; Feng, J.; Chmelka, B. F.; Stucky, G. D. *J. Am. Chem. Soc.* **1998**, *120*, 6024.
(18) Brinker, C. J.; Lu, Y.; Sellinger, A.; Fan, H. *Adv. Mater.* **1999**, *11*, 579.
(19) Huang, M. H.; Dunn B. S.; Zink, J. I. *J. Am. Chem. Soc.* **2000**, *122*, 3739.
(20) Huang, M. H.; Dunn B. S.; Soyez, H. M.; Zink, J. I. *Langmuir* **1998**, *14*, 7331.
(21) Brinker, C. J.; Scherer, G. W. *Sol−Gel Science*; Academic Press: New York, 1990; p 788.
(22) Huang, M. H.; Soyez, H. M.; Dunn B. S.; Zink, J. I. *Chem. Mater.* **2000**, *12*, 231.
(23) Ågren, P.; Lindén, M.; Rosenholm, J. B.; Swarzenbacher, R.; Kriechbaum, M.; Amenitsch, H.; Laggner, P.; Blanchard, J.; Schüth, F. *J. Phys. Chem. B* **1999**, *103*, 5943.
(24) O'Brien, S.; Francis, R. J.; Fogg, A.; O'Hare, D.; Okasaki, N.; Kuroda, K. *Chem. Mater.* **1999**, *11*, 1822.
(25) Agren, P.; Linden, M.; Rosenholm, B.; Blanchard, J.; Schuth, F.; Amenitsh, H. *Langmuir* **2000**, *16*, 8806.
(26) Linden, M.; Agren, P.; Karlson, S.; Bussian, P.; Amenitsh, H. *Langmuir* **2000**, *16*, 5831.
(27) Amenitsh, H.; Bernstorff, S., Laggner, P. *Rev. Sci. Instrum.* **1995**, *66*, 1624.

Table 1. Composition of the Initial Sols, Withdrawal Rates Used for Film Deposition, and Structures Obtained 10 min after Deposition

composition (molar ratio)				deposition rate	structure	in-plane
TEOS	H_2O	EtOH	CTAB	(mm s^{-1})	after 10 min	*d* spacing (Å)
1	5	20	0.08	2.5	*p*6*m* + wormlike	38
1	5	20	0.10	5−2.5−0.5	$P6_3/mmc$	42
1	5	20	0.12−0.14	2.5	*Pm*3*n*	39
1	2	20	0.10	2.5	*p*6*m* + wormlike	39
1	10−15	20	0.10	2.5	no organization	−

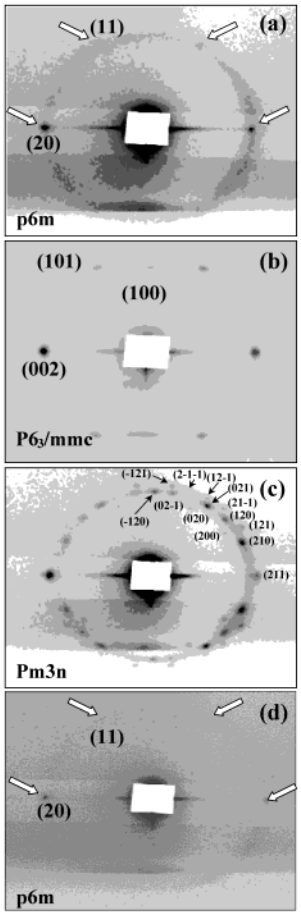

Figure 1. 2D diffraction patterns observed 10 min after deposition on films prepared with various compositions: (a) CTAB/TEOS = 0.08, H_2O/TEOS = 5; (b) CTAB/TEOS = 0.10, H_2O/TEOS = 5; (c) CTAB/TEOS = 0.12, H_2O/TEOS = 5; (d) CTAB/TEOS = 0.10, H_2O/TEOS = 2.

then withdrawn at a constant rate. A modified version of the machine was built to move the container and to keep the substrate in a fixed position. For this experiment, the substrates were very thin silicon wafers (8 μm thick) placed at an angle of 2.0 ± 0.5° with respect to the incident X-ray beam direction (grazing angle). The substrate and sol container were protected by a plastic cabinet so that the wet film could dry homogeneously. In this geometry, the X-ray beam (λ = 1.55 Å) irradiates the whole width of a fixed region of the sample. A linear detector was placed 820 mm from the sample and perpendicular to the withdrawal direction so as to collect diffracted beams induced from planes parallel to the substrate surface. The collection of the diffraction patterns started when the top edge of the beaker just passed the sample region irradiated by the X-ray beam (time T_0). At T_0 and every 100 ms thereafter, successive diagrams were collected for 3 min. A 2D diffraction pattern was then recorded on image plates in the same geometry 10 min and 1 week after deposition.

Interferometry experiments were performed using the previously described dip coater. The substrate was illuminated with a mercury lamp filtered to emit at 546 nm and placed at an angle of 20° with respect to the substrate normal. A CCD (charge-coupled device) camera (Hamamatsu Photonics) was positioned so as to record the direct reflection of the lamp from the sample surface.

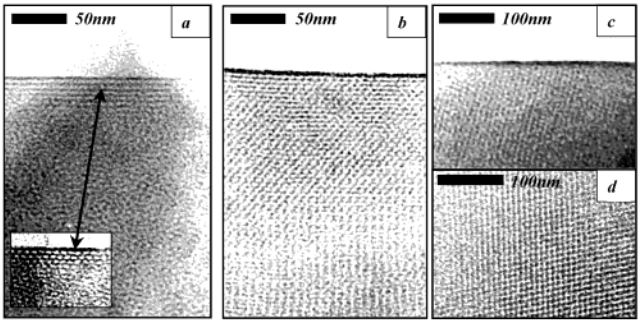

Figure 2. TEM images obtained on film cross sections: (a) film prepared with CTAB/TEOS = 0.08 showing the *p*6*m* structure at the interface and the wormlike structure in the film center, (b) film prepared with CTAB/TEOS = 0.10 and exhibiting the single $P6_3/mmc$ structure mono-oriented with the C_6 axis normal to the surface, (c) film prepared with CTAB/TEOS = 0.12 showing the mono-orientation at the air/film interface. (d) same sample as in c showing the *Pm*3*n* cubic structure with better definition.

3. Results

3.1. 2D X-ray Diffraction Investigations. Table 1 shows the experimental conditions used for each dip-coated sample, together with the corresponding structure of the as-prepared films deduced from the 2D diffraction patterns presented in Figure 1. These diffraction patterns were obtained at the SAXS beamline on films 10 min after deposition.

Depending on the sol composition, the film structures obtained were either 2D hexagonal (*p*6*m*) for CTAB/TEOS = 0.08, 3D hexagonal ($P6_3/mmc$) for CTAB/TEOS = 0.10, or cubic (*Pm*3*n*) for CTAB/TEOS = 0.12, all other parameters being equal. Figure 1a shows the 2D diffraction pattern of a film prepared with CTAB/TEOS = 0.08. The pattern is composed of a continuous ellipsoidal diffraction, corresponding to a wormlike structure, and diffraction spots (white arrows) that correspond to well-aligned 2D hexagonal domains located at both film interfaces.[28,29] These domains (a few micelle layers in thickness) can be seen on the TEM pictures of the film section in two different orientations (Figure 2a). The films were treated at 350 °C in air for 1 h before the TEM analysis, and it should be pointed out that no phase change was ever observed between the as-prepared and the heat-treated films. 2D hexagonal films with similar nanostructures have already been obtained

(28) Klotz, M.; Albouy, P. A.; Ayral, A.; Ménager, C.; Grosso, D.; Van der Lee, A.; Cabuil, V.; Guizard, C. *Chem. Mater.* **2000**, *12*, 1721.
(29) Grosso, D.; Balkenende, A. R.; Albouy, P. A.; Amenitsch, H.; Babonneau, F. *Chem. Mater.* **2001**, *13*, 1848.

by Lu et al.[7] The film obtained with CTAB/TEOS = 0.10 (Figures 1b and 2b) is composed of a single mono-oriented 3D hexagonal $P6_3/mmc$ phase. A detailed analysis of similar X-ray patterns has already been published.[10] Increasing the CTAB/TEOS ratio to 0.12, and evento 0.14, leads to films exhibiting diffraction patterns that can be precisely indexed in the $Pm3n$ cubic space group (Figure 2c). The denser (211) planes are flat-lying. The unidirectional contraction occurring during drying in the [211] direction leads to the ellipsoidal shape of the pattern. The TEM images of the film (Figure 2c and d) confirm the formation of this cubic structure and its mono-orientation. This mono-orientation of the organized domains with respect to the interfaces, observed for the cubic as well as for the 3D hexagonal phases, is related to the preferential formation of denser planes at these interfaces. Indeed, the (211) planes in the $Pm3n$ structure and the (002) planes in the $P6_3/mmc$ structure, correspond to the highest micellar density. The in-plane d spacing observed after 10 min of drying for the various films is given in Table 1. Additional X-ray analyses performed after 7 days show no change of the type organization after this long drying period. However, all of the films exhibit a further unidirectional contraction in the direction normal to the film surface (up to 15%). This phenomenon has been well explained in previous works and is mainly attributed to the slow and continuous condensation of the inorganic network.[10,12]

3.2. Influence of Experimental Conditions on Film Organization. The structure of the films (type of mesophase, extent of ordering) can be influenced by a large number of parameters, including chemical parameters (composition of the starting sol) but also processing parameters (deposition rate). In the following section, we illustrate the effect of some of these parameters on selected examples to illustrate the complexity of the formation of templated films.

Deposition Rate. The initial sol containing CTAB/TEOS = 0.10 was deposited at different withdrawal velocities ranging from 0.5 to 5 mm s^{-1}. The final structures were identical and corresponded to the 3D hexagonal $P6_3/mmc$ structure, which shows that, under our experimental conditions, the deposition rate does not affect the type of mesostructure. However, it should be pointed out that the diffraction spots recorded at lower rates were slightly better defined and more intense than those recorded at higher rates, despite the increase in thickness, and thus in diffracting matter, at the higher rates. This suggests that thinner films produced at lower deposition rates have higher degrees of organization and orientation. This effect is illustrated in Figure 3, where the profiles of the (002) diffraction peak for films deposited at 0.5, 2.5, and 5 mm s^{-1} are compared. The slight difference in the peak position is due to various extents of shrinkage.

Sol Aging Time. Figure 4 shows the XRD patterns of films produced with the same deposition rate (2.5 mm s^{-1}) and from the same sol composition (CTAB/TEOS = 0.10, H_2O/TEOS = 5) but after different sol aging times. The film prepared with the 24-h-old sol shows no organization. A broad, low-intensity peak starts to appear at d = 38 Å, 4 days after preparation of the sol. The best organization is achieved after 7 days, as shown

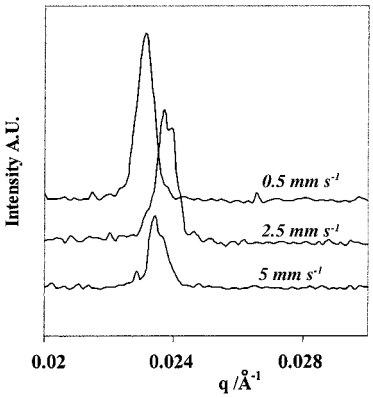

Figure 3. XRD profile of the $P6_3/mmc$ (002) peak obtained for CTAB/TEOS = 0.10 and for various deposition rates.

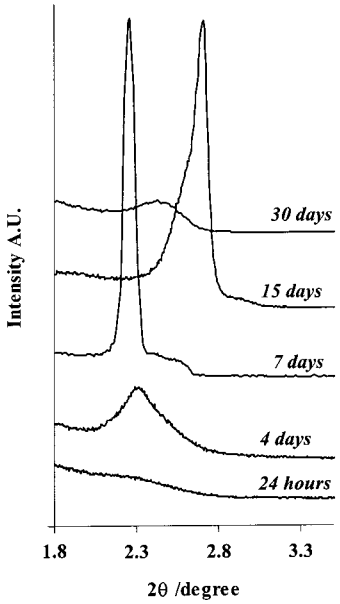

Figure 4. $\theta-2\theta$ X-ray diagrams recorded on films deposited at 2.5 mm s^{-1} from a CTAB/TEOS = 0.10 sol at different aging times. Only films between 4 and 15 days after preparation exhibit peaks that can be indexed in the $P6_3/mmc$ space group.

by the high-intensity peak centered at 39 Å. This corresponds to the $P6_3/mmc$ phase, as revealed by the 2D XRD pattern recorded at grazing incidence on this film. After 15 days of aging, the shape and position of the diffraction peak are different, suggesting that the structure might have changed from a pure $P6_3/mmc$ phase. 2D-XRD patterns were not recorded on such films which prevents an exact identification of the phase. The organization is then progressively lost with further aging as shown by the last films obtained after 30 days. A similar investigation was performed with the sol with CTAB/TEOS = 0.12, which leads to the $Pm3n$ cubic structure. The best organization was obtained for sol aged for 6 days, a result almost identical to the previous case. These delays can be reduced to a few days by slightly heating the solutions and applying a fast agitation.

The main influence of the sol aging time is on the nature of the silicate species present in solution. The composition of the sol was investigated by ^{29}Si NMR spectroscopy for the CTAB/TEOS = 0.10 solution. The relative amounts of the Q_1, Q_2, Q_3, and Q_4 units are given in Figure 5. When the solution is just prepared,

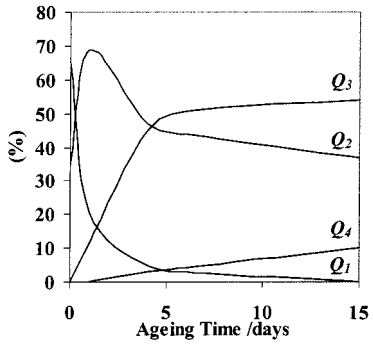

Figure 5. Aging time dependence of relative amounts of Q_1, Q_2, Q_3, and Q_4 silica species in a solution containing CTAB/TEOS = 0.10. These evolutions were deduced from the ^{29}Si liquid-phase NMR spectra by integrating and adding Q_x peaks.

most of the silicate intermediates are Q_1 and Q_2 units. After 24 h, 70% of the silicate units are Q_2, and only 10% are Q_3. After 4 days and up to a few weeks, the Q_2 and Q_3 species are in the majority. The highest degree of organization for the film seems to correspond to rather condensed species. Previous work has already shown that the condensation degree of the silica species in solution greatly influences the organization,[9] but in that case, the sol composition was different and included a higher water content ($H_2O/Si = 8.2$) and lower ethanol content ($EtOH/Si = 6.75$). In addition, the optimum of organization was reached after 200 min, and thus much faster than in our case, when only Q_1 and Q_2 species were present. Here we observe that the highest organization is achieved when species with higher degrees of condensation (cyclic and branched-linear oligomers) are formed. Even if, experimentally, it is clear that the nature of the silicate species in solution influences the final film structure, it is currently difficult to understand this phenomenon and to predict the optimum aging time for a given sol. This might correspond to an optimal charge, shape, and dimension of the inorganic intermediates for the self-assembly process to lead to a well-defined structure. An inorganic species that is too condensed will certainly lead to objects that are too large and media that are too viscous, thus preventing good self-assembly of both the organic and inorganic phases when the ethanol and water molecules have departed the layer. This aspect certainly merits further investigation.

Water Content. In addition, we have observed that the amount of water present in the initial solution, which affects the condensation degree of the inorganic intermediates, also influences the film organization. For initial solutions prepared with CTAB/TEOS = 0.10, the water content was varied between 2 and 15: the *P*6$_3$/*mmc* structure was lost when the $H_2O/TEOS$ ratio deviated from the optimal value of 5. No organization was observed for $H_2O/TEOS$ ratios greater than 5, whereas a diffraction pattern (Figure 1d) resembling the *p*6*m* and wormlike structures depicted in Figure 1a was observed for $H_2O/TEOS = 2$. The diffraction intensity, however, was quite low, suggesting either that the structure was not well organized or that only a small part of the film had the 2D hexagonal structure, with the rest being disordered.

3.3. In Situ Time-Resolved SAXS Investigation. As previously demonstrated, the organization of dip-coated templated films is a very complex process that depends on a large number of parameters. A better understanding of the formation mechanism requires the evolution of the film structure to be followed in real time when the alcohol and then the water evaporate from the wet film to yield the final solid film. Figure 6 shows the evolution of the X-ray diffraction patterns, for the three different CTAB/TEOS molar ratios (i.e., 0.08, 0.10, and 0.12) during the first 60 s that follow the deposition of wet films at $t = T_0$. The other experimental conditions are constant ($EtOH/TEOS = 20$, $H_2O/TEOS = 5$, aging time = 1 week, and deposition rate = 2.5 mm s^{-1}). The incident beam was positioned at grazing incidence, and the diffracted beams were collected on a linear detector, as depicted in Figure 7. In this configuration, the patterns correspond to the sections along the horizontal axis of the 2D diffraction patterns shown in Figure 1. The combination of a high-flux X-ray beam and a highly sensitive detector leads to high quality diffraction patterns obtained with acquisition time as short as 100 ms per diagram. The structural evolution of the film can thus be followed in real time. For silica films prepared with nonionic block copolymers as templates, similar in situ SAXS measurements have already been performed, but they used a CCD camera as the detector, which only allows patterns to be recorded every second.[29] This detector was convenient for films with relatively slow structural evolution (few tens of seconds), but not for $CTAB/SiO_2$ films, which organize much more rapidly.

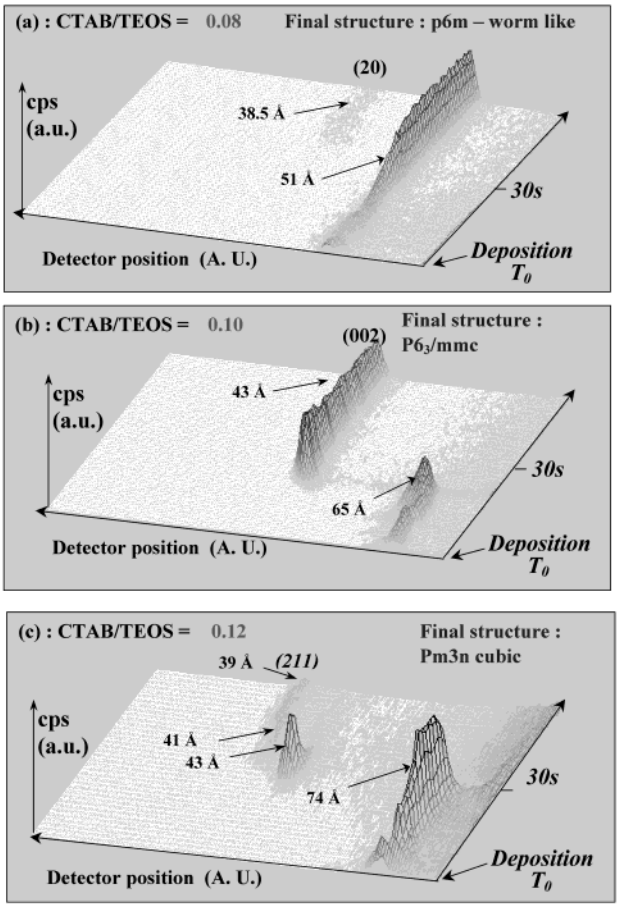

Figure 6. SAXS-determined structural evolution of the film during dip coating. The radiation wavelength was 1.55 Å. The data were collected on a linear position-sensitive detector (1 pattern every 100 ms). The initial sols were 1 week old and contained CTAB/TEOS = (a) 0.08, (b) 0.10, and (c) 0.12.

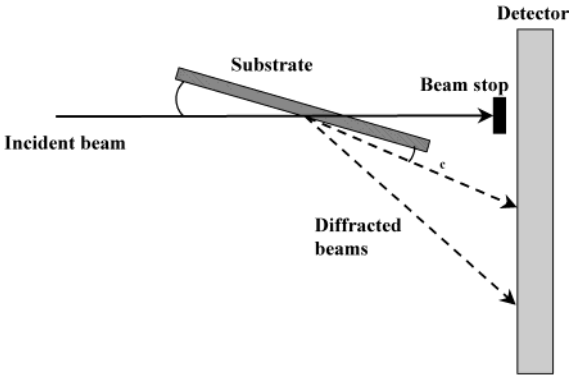

Figure 7. Diffraction geometry used in the SAXS experiments. α and α_c correspond to the angle of incidence and the critical angle of the substrate, respectively.

For the three cases presented in Figure 6a−c, one can clearly see a transient peak that starts to grow less than 1 s after T_0. It was verified that the precise location of this peak is dependent on the orientation of the substrate with respect to the incoming beam. Consequently, it probably cannot be attributed to an intermediate structure. Moreover, if it was due to an intermediate structure, then we would expect a continuous decrease of the *d* spacing, as already observed during the study by in situ SAXS measurement of the kinetics of CTAB/silicate phase behavior.[23,25] Our interpretation is that the formation of micelles leads to intense small-angle scattering that is preferentially reflected at the critical angle (see discussion section).[30,31] If this supposition is correct, then the organization of the three films appears only after a period of time that varies depending on the sample. In the case where CTAB/TEOS = 0.08 (Figure 6a), a diffraction peak corresponding to a distance of 38.5 Å starts to appear after 36 s. It corresponds to the (200) diffraction of the *p*6*m* phase formed at the interface (Figures 1a and 2a). For CTAB/TEOS = 0.10 (Figure 6b), the same phenomenon is observed, except that the diffraction peak at 43 Å attributed to the (002) peak of the $P6_3/mmc$ final structure appears sooner, after only 21 s (Figures 1b and 2b). Concerning the formation of the *Pm*3*n* cubic structure with CTAB/TEOS = 0.12 (Figure 6c), a first peak that corresponds to a *d* spacing of 43 Å appears after 26 s. It no longer exists 5 s later, and a second peak attributed to the (211) diffraction of the *Pm*3*n* final structure starts to grow after 32 s. If one considers the *d* spacing value and the high peak intensity (see below), this transient peak can be attributed to the (002) diffraction peak of the $P6_3/mmc$ structure. In this case only, the formation of the final structure seems to occur through the formation of an intermediate phase. Interestingly, one can observe that the final peak intensity is much higher for $P6_3/mmc$ than for *Pm*3*n* as a result of structure factor differences. For the *p*6*m*/wormlike film, an additional parameter that accounts for the very weak diffraction peak is the low amount of well-aligned interface.

3.4. In Situ Interferometry Investigation. During dip coating, the difference in the advancement of solvent evaporation causes the film thickness to decrease from the bottom to the top of the film at a given time. Consequently, when the film is illuminated with monochromatic light, interference fringes are observed because of the variation in thickness all along the substrate length (Figure 8a). In situ interferometry has already been used to study templated films,[18−20] and more information can be found in these papers. The observation of the interference fringes can lead to the determination of the film thickness profile with time. Constructive interferences occur at thicknesses expressed by eq 1, where *d* is the film thickness, *m* is the interference fringe number, θ is the illumination/viewing angle of the interference pattern, and *n* is the refractive index at λ = 546 nm. Destructive interferences occur at thicknesses expressed by eq 2.

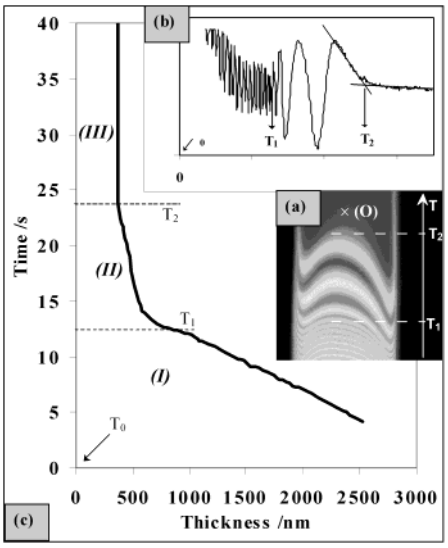

Figure 8. Interferometry data obtained for a silicon substrate withdrawn at a rate of 2.5 mm s^{-1} from a 1-week-old sol containing CTAB/TEOS = 0.12: (a) interferometry frame showing T_1 and T_2, the three different regimes, and the position of analysis (O); (b) time profile of the fringe intensity at O; (c) evolution of the film thickness with drying time.

$$d = \frac{m\lambda}{2n\cos\theta} \quad (1)$$

$$d = \frac{(2m+1)\lambda/2}{2n\cos\theta} \quad (2)$$

On the basis of the thickness of the final film deduced from spectroscopic ellipsometric measurements performed at an incidence angle of 75°, the number *m* of the last observable fringe can be easily determined. A sequence of interference patterns (10 images per second) was recorded at a fixed location (O in Figure 8a) far from the film edges during deposition. For better understanding, the horizontal scale in this figure was transformed from distance into time, using the known deposition rate. Variation of the reflected light intensity can then be plotted versus time (Figure 8b). Using the fringe number in eqs 1 and 2 leads to film thickness profiles with time (Figure 8c). The variation of the refractive index was considered to be linear between 1.36 for the sol and 1.47 for the dry film. To compare the time evolution of the film thickness deduced by interferometry with the structure evolution deduced by SAXS,

(30) Babonneau, D.; Petroff, F.; Maurice, J.-L.; Fettar, F.; Vaures, A.; Naudon, A. *Appl. Phys. Lett.* **2000**, *76*, 2892.
(31) (a) Sinha, S. K.; Sirota, E. B.; Garoff, S.; Stanley, H. B. *Phys. Rev. B* **1988**, *38*, 2297. (b) Weber, W.; Lengeler, B. *Phys. Rev. B* **1992**, *46*, 7953.

every effort was made to perform the deposition under the same experimental conditions (dip-coating conditions, sol composition and age, initial T_0, and analyzed film area).

Figure 8 was obtained with a sample deposited at a rate of 2.5 mm s^{-1} from a solution containing CTAB/TEOS = 0.12. The final structure of the film is $Pm3n$ as previously discussed. Three specific times are indicated in this figure. T_0 corresponds to the time when the top level of the solution passed the analyzed point (O), whereas T_1 and T_2 represent the times when the rate in the thickness evolution changed, which corresponds to variations in the evaporation rates measured at O. One can observe that three different regimes occur consecutively during drying. The first regime between T_0 and T_1 (first 13 s) is fast and is attributed to the rapid evaporation of mainly ethanol. The second regime between T_1 and T_2 (from 13 to 24 s) is slower, due primarily to the departure of water. The third regime starts after T_2 and is due to the loss of residual water and ethanol molecules adsorbed in the solid film, as well as those arising as byproducts of the condensation of the silica network. In this particular case, the film has a thickness of 310 nm at 25 s and of 305 nm 10 min later, suggesting that the third regime of evaporation does not create a significant contraction. T_2 corresponds to the drying line, as the evaporation is considered to be negligible after T_2. These results are consistent with the recent work published by Huang et al.,[19] which shows by in situ luminescence probing and for similar systems, that the maximum content of water is reached before the drying line.[32] Solutions with various compositions were used to produce films, and the interferometry investigations led to similar film thickness profiles versus time. They all showed three different evaporation regimes. Increasing the water content only increased the duration of the second regime. On the other hand, T_1 and T_2 were unchanged when the ratio of CTAB/TEOS was changed from 0 to 0.14, suggesting that the presence of CTAB does not noticeably affect the evaporation process.

3.5. Comparison between SAXS and Interferometry Results: Influence of the Deposition Rate. For the first time, in situ SAXS and interferometry experiments have been combined to contribute to a better understanding of the film formation mechanism. The system with CTAB/Si = 0.10, which leads to the $P6_3/mmc$ structure, was chosen for this study. The different characteristic times T_0 (- -), T_1 (▲), and T_2 (■) were deduced from interferometry. They are reported in Figure 9 for films deposited at various rates (i.e., from 0.5 to 5 mm/s). All of the films show the $P6_3/mmc$ hexagonal structure according to 2D XRD. The time at which the diffraction peak characteristic of this phase appears during the in situ SAXS experiment [T_H (●)] is also reported. As expected, T_1 and T_2 increase with deposition rate as the amount of liquid dragged from the solution is larger at higher rates. At a low rate (0.5 mm s^{-1}), film organization occurs 10 s after T_2, that is, when the film thickness is practically established. At the intermediate rate of 2.5 mm s^{-1}, this period is reduced to 3 s, and at the highest rate of 5 mm s^{-1}, T_H is almost equal to T_2. These results suggest that the formation of the $P6_3/mmc$ phase occurs in the final stage of film evaporation close to the drying line. The period separating the drying line (T_2) from the onset of organization (T_H) is greater for lower deposition rates and, therefore, for thinner films. Another way of interpreting this observation is to say that the shorter the second evaporation regime, the longer the period needed for the film to organize.

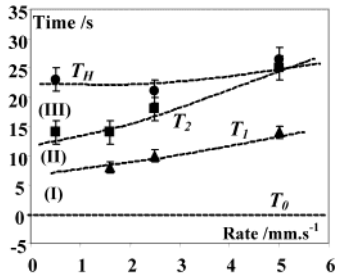

Figure 9. Evolution of T_0, T_1, T_2, and T_H for deposition of the 1-week-old sol containing CTAB/TEOS = 0.10 at various rates. The dotted lines are drawn as guides for the eyes.

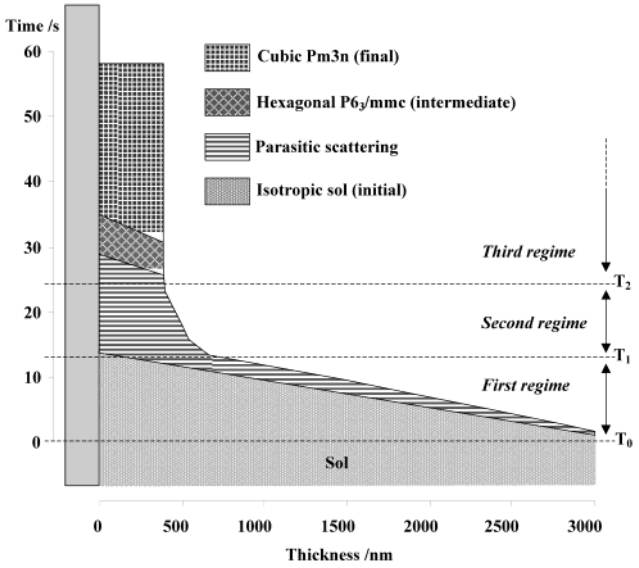

Figure 10. Structural evolution of a film deposited at 2.5 mm s^{-1} from a sol with CTAB/TEOS = 0.12 versus time and film thickness. The formation of the final cubic $Pm3n$ structure occurs through the formation of a $P6_3/mmc$ intermediate phase.

4. Discussion

We have clearly shown that the formation of highly oriented mesostructured silica films is a complex process in which the initial concentration of surfactant, the rate of evaporation, the degree of polycondensation of the silicate species, and the composition of the liquid phase all influence the organization. Moreover, the formation of films by dip coating involves a rapid evaporation process and, in certain cases, the formation of intermediate phases. In the following section, we discuss the different steps involved in film formation using a combination of the results obtained by in situ SAXS and interferometry measurements (see Figure 10).

4.1. The First Scattering Peak. In all of the films studied by in situ SAXS, a transient peak was detected from the beginning of the process. As reported by Yang et al.[4] for the growth of templated silica films at the

(32) Brinker, C. J.; Frye, G. C.; Hurd, A. J.; Ashley, C. S. *Thin Solid Films* **1991**, *201*, 97.

air/water interface the micelles interact with air to form a first layer of organized micelles at the interface, when the concentration of surfactant is high enough. According to the CTAB/EtOH/H_2O phase diagram, spherical micelles are present at concentrations above the CMC (critical micelle concentration) only in pure water. In the presence of ethanol, the first reported micellar cell is a bidimensional hexagonal one, suggesting that the formation of cylindrical micelles is favored in such an environment.[33] For the present systems, where the medium is mostly alcoholic before T_1, we can *suppose* that, early in the evaporation process, the formation of micelles at the air/film interface leads to this intense small-angle scattering preferentially reflected at the critical angle,[30,31] whatever the incident angle. Here, the variable peak position observed for the three different samples is due to the experimental error made when the substrate angle is adjusted. The presence of such off-specular diffuse scattering can be attributed to the roughness of the interface and indicates that the surface of the film is somehow disturbed. We can also imagine that these micelles do not organize at random and might be stacked almost parallel to the interface to produce such an effect. It is clear that this transient peak contain information on the early stages of the film formation, and its origin will be investigated in more detail soon. The peak intensity increases during evaporation. If one assumes that this peak is related to the micelles, then this increase in intensity can be attributed to the formation of micelles induced by the global increase in the surfactant concentration close to the interface enhanced by the departure of ethanol. This transient peak appears for any composition. For cubic and 3D hexagonal films (i.e., CTAB/TEOS = 0.12 and 0.10, respectively), the peak progressively disappears with the formation of the 3D mesostructures. On the other hand, for 2D hexagonal films (i.e., CTAB/TEOS = 0.08), it remains intense, which suggests a rougher surface.

4.2. Formation of the Mesostructures. We have shown that three different structures, formed by the arrangement of two possible types of micelles (i.e., spherical or cylindrical), can be obtained via a slight variation of the CTAB content (0.12 ≥ CTAB/TEOS ≥ 0.08). By increasing the CTAB/TEOS ratio, we observed first the *p*6*m*, followed by the $P6_3/mmc$, and then the *Pm*3*n* structures. Honma et al. reported a somewhat different order for 0.25 ≥ CTAC/TEOS ≥ 0.093 that was first 1D hexagonal, followed by the bicontinuous *Pn*3*m* and then lamellar structures.[16] According to the SAXS results obtained with our system, the formation of the *Pm*3*n* structure seems to occur through the formation of the $P6_3/mmc$ mesostructure, that can here be considered as an intermediate phase. For sol compositions richer in water, it seems that the final film structure can be predicted from the water/surfactant binary diagrams.[34] With our experimental conditions (ethanolic sol), however, the evolution of the micelle morphology and the mesophase cannot be predicted by taking into account only the CTAB concentration, even if it appears to be a very critical parameter. Indeed, the fact that the medium and the concentrations are constantly changing during evaporation/drying (consequently varying the interactions at the micelle interfaces) strongly complicates the comprehension of the film formation mechanism.

Formation of 3D Hexagonal and Cubic Phases. In Figure 10, one can see that these phases appear a few seconds after T_2, and thus close to the drying line, when the medium is no longer aqueous but mainly composed of around 40 wt % of surfactant and 60 wt % of a relatively condensed silica gel. These percentages were evaluated from the initial and final film compositions and the evolution of the film thickness. In view of the wormlike structure obtained with the lower CTAB/TEOS ratio of 0.08, the micelles are expected to have elongated spaghetti-like shapes when they are first formed in the evaporating film. The $P6_3/mmc$ and then *Pm*3*n* structures cannot be formed by the assembly of such elongated micelles but require more spherical-like discrete micelles. The transformation from elongated to spherical micelles must thus occur before or at the drying line and is accompanied by an increase in the micelle curvature radius. This morphological transformation should be related either to the change from ethanol-rich to water-rich medium when the film is still liquid or to the final stage of water evaporation.

The organization of the micelles first into the $P6_3/mmc$ structure takes place after this transformation and after the drying line, suggesting that it is mainly due to the self-assembly of CTAB with the inorganic intermediates. When CTAB/TEOS ≥ 0.12, the $P6_3/mmc$ structure is unstable and transforms into a cubic *Pm*3*n* structure after a few seconds of existence via a rearrangement of the micelles. As for the formation of the first $P6_3/mmc$ structure, this phase transition is rapid but lasts for a few seconds, suggesting that composition gradients still exist within the film after 30 s. The mechanism involved in such a lattice transformation (3D hexagonal structure into cubic structure) is not yet understood. However, it is evident that this transformation is observed only for CTAB concentrations higher than 0.10. The transformation is thus attributed to the difference in charge density matching at the micelle interfaces induced by the difference in surfactant concentrations. During the hours that follow this phase formation, the film inorganic network continues its drying/polycondensation as shown by the 2% thickness reduction observed after 10 min.

Formation of the P6m Structure at the Film Interfaces. For the structure obtained with CTAB/TEOS = 0.08, two types of domains must be considered: wormlike at the center and well-aligned *p*6*m* 2D hexagonal at the interfaces. We suggested that the first micelles adopt an elongated micellar shape. Both *p*6*m* and wormlike structures are based on elongated micelles. In the wormlike domains, these micelles are randomly organized. Such a structure is often observed in poorly organized systems, and its formation can be attributed to the lower concentration of CTAB in the initial solution. The XRD peak appearing after 36 s is a Bragg peak obtained by diffraction from planes that are parallel to the interface and thus due to the *p*6*m* well-aligned domains. We propose that the well-aligned *p*6*m* structure present only at the film/air interface results from the influence of the interface with air on the wormlike structure. When evaporation of the liquid

(33) Fontell, K.; Khan, A.; Lindstrom, B.; Maciejewska D.; Puang-Ngern, S. *Colloid Polym. Sci.* **1991**, *269*, 727.

(34) Klotz, M.; Idrissi-Kandri, N.; Ayral, A.; Guizard, C. *Mater. Res. Soc. Symp. Proc.* **2000**, 62, CC7.4.1.8.

phase is completed after T_2 (the film thickness no longer varies), micelles located at the interface are forced to align parallel to the surface. This rearrangement is then transmitted to the closest micelles underneath the surface creating a locally well-organized layer with a thickness of a few micelles (Figure 2a). The reorganization stops when the inorganic network becomes too rigid. Such a phenomenon has been studied in detail for other systems of mesostructured films and is discussed separately.[29]

4.3. Phase Formation versus Drying Line and Evaporation Rate. In Figure 9, we show that the time at which the first 3D $P6_3/mmc$ structure appears seems to be independent of the deposition and evaporation rates. However, it seems to take place after the drying line. In this section, we examine the influence of the evaporation rate, which is associated with the withdrawal speed and the film thickness, on the degree of organization. The drying of a thicker film requires more time because of the greater quantity of liquid and solid phase deposited. As a result, both the first and second evaporation regimes last longer (T_1 and T_2 increase) for thicker films produced at higher withdrawal rates. On the other hand, Figure 9 shows that the time at which the mesostructure forms (T_H) is not dramatically influenced by the deposition rate and the film thickness and that it tends to occur later after the drying line, especially for low deposition rates. Acid-catalyzed condensation of organosilicate precursors leads to polymeric gels that are formed by percolation of fractal lacunar aggregates.[35] This inorganic system composed of sufficiently uncondensed species seems appropriated for allowing rearrangement within the film after the solvent has evaporated. The fact that thinner films exhibit better organization suggests that rapid solvent evaporation promotes good self-assembly, in agreement with previously published work.[19] One can also argue that, in thinner films, the effects of surface energy are relatively more important than those of evaporation rate, because a higher fraction of the film volume is near the interface.

Another point that emphasizes the uniqueness of the evaporation-induced self-assembly process is that, to our knowledge, mesostructured silica powders with $P6_3/mmc$ and $Pm3n$ geometries have never been produced with CTAB, whereas we obtained them with a high degree of organization as films. In the case of powders, two other types of surfactant are required.[36] Furthermore, in the case of films, three types of structure can be produced under the same experimental conditions with only a slight change in the CTAB/TEOS ratio. Therefore, the liquid deposition method used to produce films leads to a greater variety of structures for a given system than the method used to produce powder.

5. Conclusion

This work has demonstrated that highly organized mesostructured silica films with different structures can be obtained by dip coating using CTAB as the templating agent. Under the chosen experimental conditions, the key parameter for adjusting the final structure is the CTAB/Si molar ratio. Different porous networks can be obtained—3D hexagonal ($P6_3/mmc$), cubic ($Pm3n$), and columnar hexagonal ($p6m$)—that have been identified by coupling two-dimensional X-ray diffraction at grazing incidence and TEM investigations on film cross sections. The ability to tune the pore geometry and connectivity makes this synthetic approach quite promising for applications that require different porous network topologies. We have also shown that the extent of film organization depends on the aging of the starting solution. An optimal condensation degree seems to exist for the silicate species, which indeed varies depending on the ethanol and water contents of the initial solution. This factor is currently difficult to analyze but might be related to a certain morphology and surface charge of the inorganic intermediates that are well adapted for association with the CTAB surfactant.

To obtain a better understanding of the mechanism of film formation, an in situ SAXS analysis of the structural evolution of these films during dip coating was performed even when the film formation occurred in less than 1 min under the chosen experimental conditions. A high-flux synchrotron X-ray beam was used, and the high degree of organization of the films allowed us to use acquisition times as short as 100 ms for each X-ray diffraction patterns. The total evolution of the structure during drying could thus be followed in real time. For the first time, these SAXS investigation were combined with in situ interferometry measurements to correlate changes in the structure with the evolution of the film thickness. Several steps in the film formation were found experimentally, and a model was proposed that implies (i) the formation of micelles at the film/air interface, (ii) a morphological change of the micelles for the formation of both hexagonal and cubic 3D structures, and (iii) the existence of the intermediate 3D hexagonal phase for the formation of the specific $Pm3n$ cubic structure. Very interestingly, the final organization takes place at a later stage in the film evaporation process and even up to a few seconds after the drying line for lower deposition rates. At this stage, the headgroups of the surfactant are mainly in interaction with the silicate oligomeric moieties.

This paper has clearly demonstrated the complexity of the evaporation-induced self-assembly process for preparing mesostructured silica films using a cationic surfactant. The large number of parameters that influence the structural evolution of the films makes a fundamental understanding of the film deposition chemistry and physics difficult to obtain. The effort to combine in situ measurements with fast response using techniques such as SAXS, interferometry, and also luminescence probing[19] should be continued to obtain a better understanding of film formation and, thus, a better control of the final film properties.

Acknowledgment. The authors acknowledge the financial support of Philips Research (Eindhoven, Netherlands). The European Commission also greatly contributed to this study by supporting our access to the ELETTRA synchrotron (EU Large-Scale Facility).

CM011255U

(35) Brinker, C. J.; Scherer, G. W. *Sol−Gel Science*; Academic Press: New York, 1990; p 108.
(36) Huo, Q.; Margolese, D. I.; Stucky, G. D. *Chem. Mater.* **1996**, *8*, 1147.